Hindawi
Geofluids
Volume 2023, Article ID 7316335, 14 pages
https://doi.org/10.1155/2023/7316335

Research Article

The Combined Effect of Nanoclay Powder and Curing Time on the Properties of Class G Cement

Abdulmalek Ahmed, Ahmed Abdulhamid Mahmoud, and Salaheldin Elkatatny

College of Petroleum Engineering and Geosciences, King Fahd University of Petroleum & Minerals, 31261 Dhahran, Saudi Arabia

Correspondence should be addressed to Ahmed Abdulhamid Mahmoud; ahmed.mahmoud@kfupm.edu.sa and Salaheldin Elkatatny; elkatatny@kfupm.edu.sa

Received 24 August 2022; Revised 12 July 2023; Accepted 17 November 2023; Published 21 December 2023

Academic Editor: Azizollah Khormali

When the cement paste is subjected to stresses, the cement matrix and its characteristics are dramatically influenced, especially in the early ages of cement hydration when the cement properties have not yet settled. Nanoclay, which is made up of very small particles, was used to improve the properties of cement. In this study, the early-age performance of cement made with nanoclay powder for use in oil wells is assessed. Ten cement samples were made and cured at varying times (6, 12, 24, 48, and 72 hours), wherein 1% by weight of cement of nanoclay was used in five samples, and in the other five samples, there was no nanoclay present in the cement. Failure properties, petrophysical parameters, and elastic properties were studied for all the cement samples. Nuclear magnetic resonance (NMR), X-ray diffraction (XRD), and scanning electron microscopy (SEM) were all used to describe the cement samples and determine how different curing times affected the cement's mineralogical and microstructural features. The results displayed that compressive and tensile strengths were shown to increase with curing time for both the base (control) and nanoclay cement samples; however, the compressive and tensile strengths of the nanoclay cement samples were found to be greater than the base sample by 20.2% and 17.9%, respectively. This is due to the presence of more calcium silicate hydrate in these samples. Nanoclay cement had 76.9% lower permeability than control cement, which can be related to the capacity of the nanoclay particles to fill the microstructure dominating the base samples as curing time increased. Young's modulus of the cement was lowered by 1.8%, while Poisson's ratio was increased by 2.7% when nanoclay was incorporated. Nanoclay cement has a 29.2% smaller porosity than regular cement, and this porosity increases as the cement cures. The novelty of this work is that several properties of the class G cement were evaluated at the early stage of hydration, where the nanoclay particles were used to improve these properties.

1. Introduction

Cement slurries are poured into the annulus when the steel casing is used to withstand the stresses of collapse and burst [1]. As the slurry gradually hardens, it forms the cement sheath. The cement sheath plays a critical role in maintaining the integrity of the well by preventing fluid movement between different formations, ensuring zonal isolation, protecting the casing string from corrosion, and providing mechanical support to both the casing and the drilled zones. In the event of a worst-case scenario, the deterioration of the cement paste can lead to pressurization within the annulus, migration of formation fluids to the surface, and potentially even a blowout. Developing a high-performance cement paste that ensures the fundamental integrity of the well and reduces the risk of failure caused by the accumulation of materials resulting from physicochemical processes can help mitigate the potential for cement failure [2].

Many scientists have recently analyzed the feasibility of using nanoparticles to enhance the properties and performance of cement slurries, lengthen the well's useful lifespan, and reduce costs caused by cement matrix failures, for example, incorporating nanosilica with oil-well cement for improving the pozzolanic reaction of cement [3–7], enhancing the cement's early age strength, and reducing the permeability of the cement matrix [2, 8, 9]. Nanosilica was also

used with nanoalumina to increase the cement's compressive strength [10–12]. Xu et al. [13] looked into the effects of adding nanosilica to cement and found that, when mixed with traditional dispersants, the cement's rheological and mechanical qualities improved. According to the research of McElroy et al. [14], the optimal concentration of nanoalumina fiber for the formation of the maximal compressive strength of cement is 0.1%. The application of carbon nanotubes and nanozeolite in oil well cementing was also investigated by several authors [15, 16]. Carbon nanofiber combined with other nanomaterials has been shown by Dinesh et al. [17] to enhance the self-sensing characteristics of cement and aid in keeping the cement sheath compact. In addition to being resistant to microcracks, carbon nanofibers have improved strength, Young's modulus, fatigue resistance, and ductility. Ren et al. [18] studied the synergetic impact of nano-SiO_2, nano-TiO_2, and nano-$CaCO_3$ and found that the optimum doses of NS, NT, and NC are 0.86 wt%, 2.75 wt%, and 0.14 wt%, respectively. Wang et al. [19] suggested using nano-SiO_2, ultrafine fly ash, and polycarboxylate superplasticizer to address some issues related to the released heat during the hydration reaction. The combined power of these additives makes it possible to finely modulate hydration processes.

Because of their high aspect ratio, pozzolanic nature, and low cost, lamellar nanoparticles like clays are of particular interest among the various nanoparticle types [20]. Nanoclay is a very fine-grained material that occurs naturally and develops plasticity once it is mixed with water. Many different fields have found new uses for nanoclay, which is both common and environmentally friendly. Nanoclay can be easily modified by adding organic or inorganic agents due to its accessible layer structure [21]. Nanoclay has a very small particle size that enables it to fill the microporous in the cement matrix which will increase the strength of the cement [22, 23]. This feature of the small size can also increase the solidified cement matrix density besides the large surface area of nanoclay that helps in accelerating the reactions throughout the hydration process of the cement and densifying the matrix's microstructures [24–26]. Nanoclay's potential as an oil-well cement additive has been greatly increased by its many advantageous properties. Therefore, many researchers used nanoclay to improve the oil-well cement properties [27–29]. Ma et al. [30] and Ma and Kawashima [31] used nanoclay to investigate the effects of pressure and temperature on the rheological characteristics of cement slurries. Tariq et al. [32] investigated the impact of temperature on cement slurry design utilizing nanoclay particles. Cement's rheological characteristics and mechanical strength benefit from an increase in temperature. When added to cement, NCs reduce porosity and permeability by filling the pores at a higher temperature. Mohammed [33] found that as the concentration of nanoclay increased from 0% to 1%, the yield stress and plastic viscosity of cement slurries increased by 5%–65% and 3%–16%, respectively. Compressive strength improved by 12% after one day and 43% after 28 days for the oil well cement.

Through the hydration process, cement paste transforms from a fluid to a solid. Cement paste properties are dependent on the composition of the cement, (w/c) ratio, other materials' properties, and conditions of curing time such as temperature, pressure, and the fluids contacting the cement matrix [34, 35]. Further, the cement sheath is subjected to a number of loadings over the well's lifetime, which may affect the cement sheath's properties [36]. Those loadings are related to many reasons such as fracture formation, mechanical stress, thermal loads, poor casing centralization, geochemical attack, hydraulic fracturing, water loss, cement shrinkage, inadequate cement bond, inadequate drilling mud removal, and contamination. It is possible to reach pressures of over 40 MPa when drilling the well and a varying pressure from 10 MPa to 80 MPa when testing the integrity of the well's casing [37]. The application of external forces can result in the cement sheath deforming, which may cause cracks to form at the junction between the casing-cement or rock-cement interfaces. This effect becomes more pronounced when these forces are exerted in the initial stages of the curing process, prior to the cement attaining its complete mechanical properties and strength. Commonly, well leaks are frequently associated with the contraction of cement and the premature decrease in pore pressure [38–40].

Limited research has been carried out to study the hydration process of wellbore cementing under challenging conditions and different curing durations. The existing investigations have mainly focused on elastic and mechanical properties [41]. However, the consequences of the change in properties due to the development of the hydration process were not investigated. When looking at the cement sheath's early age properties, there are a few different experimental approaches to perform. Some of these techniques analyze the cement's reaction rate, while others analyze the cement's chemical or physical properties at various times [42, 43]. For example, Ahmed et al. [44] investigated the impact of adding polypropylene fiber to class G oil well cement on its curing time and various properties. The study found that the addition of polypropylene fiber enhanced the cement's strength, reduced porosity and permeability, and increased elasticity. Various experimental techniques were used to assess the properties of the cement samples at different curing times, and the results consistently showed improvements in compressive and tensile strength, reduced permeability and porosity, and increased Young's modulus. The study also revealed relationships between these properties and curing time, which were accurately modeled by mathematical equations.

In this study, several properties of the nanoclay cement and the base (control) cement (without nanoclay) were evaluated throughout the first phases of hydration. Compressive and tensile strengths, porosity, permeability, Poisson's ratio, and Young's modulus were measured at 6, 12, 24, 48, and 72 hours of curing. To investigate how cement qualities vary over time, nuclear magnetic resonance (NMR), X-ray diffraction (XRD), and scanning electron microscopy (SEM) were applied to cement samples.

2. Methodology

2.1. Materials. Class G cement and nanoclay are the main components in this work, together with a number of

Table 1: Information of the used class G cement and nanoclay.

	Class G cement	Nanoclay
Specific gravity	3.15	1.98
D_{10} (μm)	3.7	2.5
D_{50} (μm)	20.9	9.7
D_{90} (μm)	40.6	20.8
Main elements	Ca = 70%, Si = 12%, and Fe = 9%	O = 49%, Si = 32%, and Al = 12%
Surface area (m^2/kg)	340	657

chemical additives (silica flour, deformer, dispersants, fluid loss agents, and so on) utilized to improve cement performance and make them applicable to a variety of wellbore conditions. Based on the results of X-ray diffraction (XRD), the class G cement utilized in this work is composed of the following chemicals: $(C_3S) = 65\%$, $(C_2S) = 15\%$, $(C_4AF + 2C_3A) = 18\%$, and $(C_3A) < 1\%$. The specific gravity of the used class G cement was found to be 3.15.

The nanoclay employed here is a modified form of montmorillonite that has a high surface area and a low specific gravity of 1.98. It may accelerate the cement's hydration kinetics of the cement by encouraging the precipitation and nucleation methods of C-S-H as a mass during the first phase of the hydration [45, 46]. Class G cement used in the study was provided by a service company, and the nanoclay was supplied by another Saudi-based chemical company.

Table 1 summarizes the properties of class G cement and nanoclay used in this study. The information in Table 1 was obtained from the labs using different equipment such as an automatic density analyzer, particle size analyzer, and X-ray fluorescence (XRF).

Using the ANALYSETTE 22 Nano Tec plus wet dispersion unit, the particle size distribution (PSD) of the class G cement and nanoclay particles was determined. Figure 1 displays the results, which show that the average cement's size is 20.9 μm, significantly larger than the average size of nanoclay, which is 9.7 μm.

The X-ray fluorescence (XRF) analysis of class G cement and nanoclay reveals that nanoclay contains significantly more oxygen and silicon than cement (about 49% and 32%, respectively). Figure 2 shows that while cement contains a lot of calcium (72%), nanoclay contains only 5%. In addition, it is shown that nanoclay has a good amount of aluminum and iron, at 12% and 6%, respectively. The M4 TORNADO instrument, which utilizes the small-spot micro X-ray fluorescence technique, was employed for X-ray fluorescence (XRF) analysis to determine the elemental compositions. Powdered samples were utilized, and the elemental detection was carried out using a MicroXRF instrument (Bruker). This instrument was equipped with a microfocused Rhodium source (50 kV, 600 μA) and a polycapillary optic that generated a spot size of around 20 μm. To quantify the elemental intensities from the spectral data, the obtained elemental spectra of the samples were processed using proprietary M4 software.

2.2. Experimental Program. Cement slurries were made using methods prescribed by the API standards [47, 48]. Class G cement, fluid loss additive at 0.7% by weight of cement to control the leakage of the aqueous phase of the cement, 35% silica flour, 0.1% expandable material, 0.08% dispersion, 2.82 10^{-6}% defoamer, and 44% water were used in making the base cement (without nanoclay). The main compounds of fluid loss, silica flour, dispersion, and defoamer are calcium hydroxide, crystalline silica, sulfonic acid salt, and hexadecane, respectively. The nanoclay cement slurry was created by combining another new slurry with 1% of nanoclay and the additives originally contemplated for the control slurry. Based on the recommendation of Murtaza et al. [28], 1% of nanoclay was used.

Each slurry was then poured into a mold of the appropriate size (cubes of size $(2 \times 2 \times 2$ inch$^3)$ and cylinders of 4.0 inches in height and 1.5 inches in diameter) before undergoing the necessary tests. Next, the molds were placed in a water bath preheated to 170°F and left the samples to cure for 6, 12, 24, 48, and 72 hours. The failure tests, petrophysical tests, elasticity tests, density variation, NMR, and XRD were performed at each curing period on the base and nanoclay cement specimens. The experimental program is summarized in Figure 3.

2.2.1. Mechanical Tests. At various curing times, the samples were tested for their compressive and tensile strengths. The compressive strength of the cement was measured using cubes with 2.0-inch edges in accordance with ASTM [49]. The Brazilian tensile test was performed following ASTM standard [50], and samples were 1.5 inches in diameter and 0.75 inches in length. During the tests, the samples were loaded at a constant rate of 1.5 KN/sec. All measurements were performed three times, and the reported values represent the average strength out of the three measured values.

2.2.2. Petrophysical Tests. To explore how the petrophysical properties of the nanoclay specimens are affected by the duration of curing, the porosity and permeability of all samples were examined at varying curing intervals. Petrophysical parameters were assessed using samples measuring 1.5 inches in diameter and 1.0 inches in thickness. The automated porosimeter-permeameter was employed to measure both the permeability and porosity of the samples. The automated permeameter-porosimeter (AP-608) from Coretest System Inc was used. Boyle's law and Klinkenberg's effect were implemented to measure the porosity and permeability, respectively. Helium gas was utilized as pore fluid to obtain the porosity and permeability of the cement samples. Confining pressures ranging from 900 to 1300 psi were applied in the measurement at room temperature.

2.2.3. Nuclear Magnetic Resonance. To investigate how curing time affected the pore size distribution and porosity changes of the nanoclay and control specimens, a low magnetic field (2 MHz) NMR spectroscopy system "Geospec rock analyzer" from Oxford Instrument was used. All cement samples were subjected to NMR in order to analyze the effects of porosity variation on the pore size distribution.

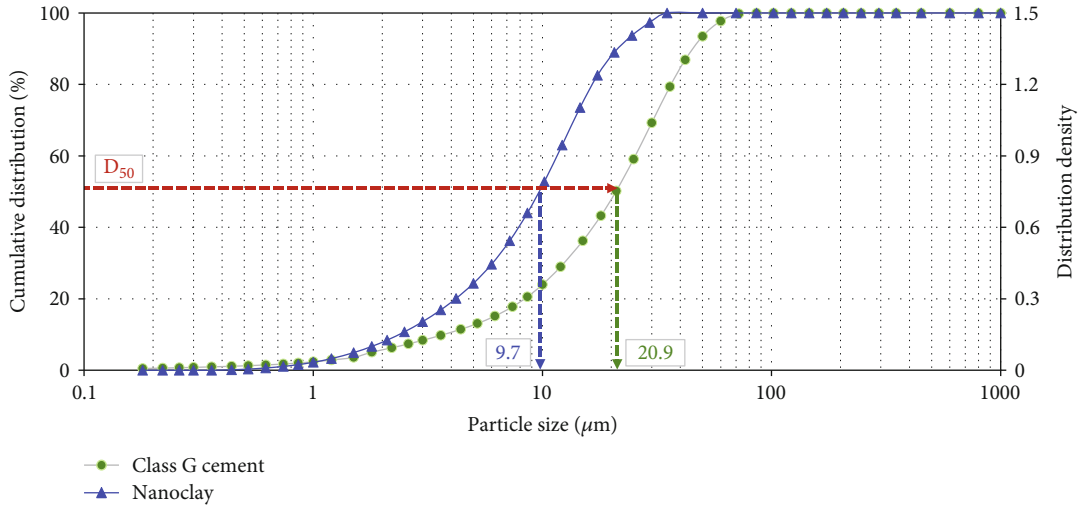

Figure 1: PSD of (a) class G cement and (b) nanoclay.

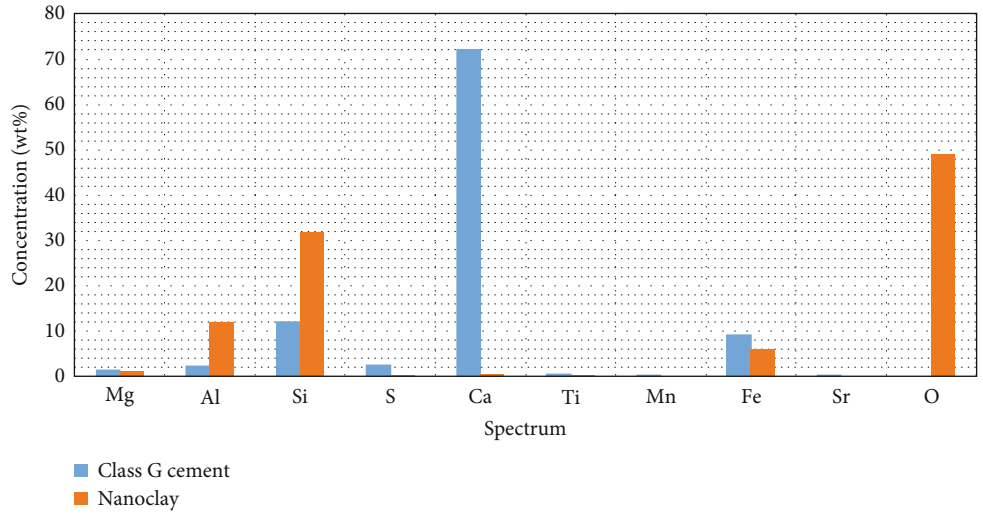

Figure 2: The composition of class G cement and nanoclay.

The relaxation time (T_2) was measured by nuclear magnetic resonance (NMR) with a weak magnetic field, which easily causes nuclear spin-precession that can be detected, on 1.5-inch-diameter by 4.0-inch-long cylinders of cement samples. The PDF and CDF for the full length of the cement specimens (4 inches) were plotted.

2.2.4. Elasticity Test. To assess the properties of all cement samples, Young's modulus and Poisson's ratio were measured using cylindrical specimens measuring 4.0 inches in length and 1.5 inches in diameter. The elastic properties were determined through the utilization of sonic velocities, specifically compressional and shear waves. The elasticity test was conducted using an ultrasonic device integrated into the Wombat Epslog scratch machine. This device consists of two probes, a transmitter and a receiver, which enable the emission and recording of both bulk and shear waves. The probes are positioned 4 cm apart, and the time taken for a pulse to travel between them is recorded. By calculating the compressional and shear velocities, derived from the recorded time, the dynamic Poisson's ratio and dynamic Young's modulus can be determined.

2.2.5. Mineralogical Composition and Microstructural Analysis. The impact of curing time on the hydration products and microstructure of both the base (control) and nanoclay cement samples was analyzed using X-ray diffraction (XRD) and scanning electron microscopy (SEM). Specifically, XRD was employed to investigate how the composition and structure of the cement changed within the initial three days of curing.

For the XRD analysis, the raw data was processed and quantified using the Rietveld method and HighScore Plus software. Spectra were obtained using a Malvern PANalytical EMPYREAN Diffractometer system, with a 2θ range from 4° to 70° and a step size of 0.01°. The step size indicates the incremental increase in angle considered during each measurement step. The XRD equipment utilized a Pixcel1D

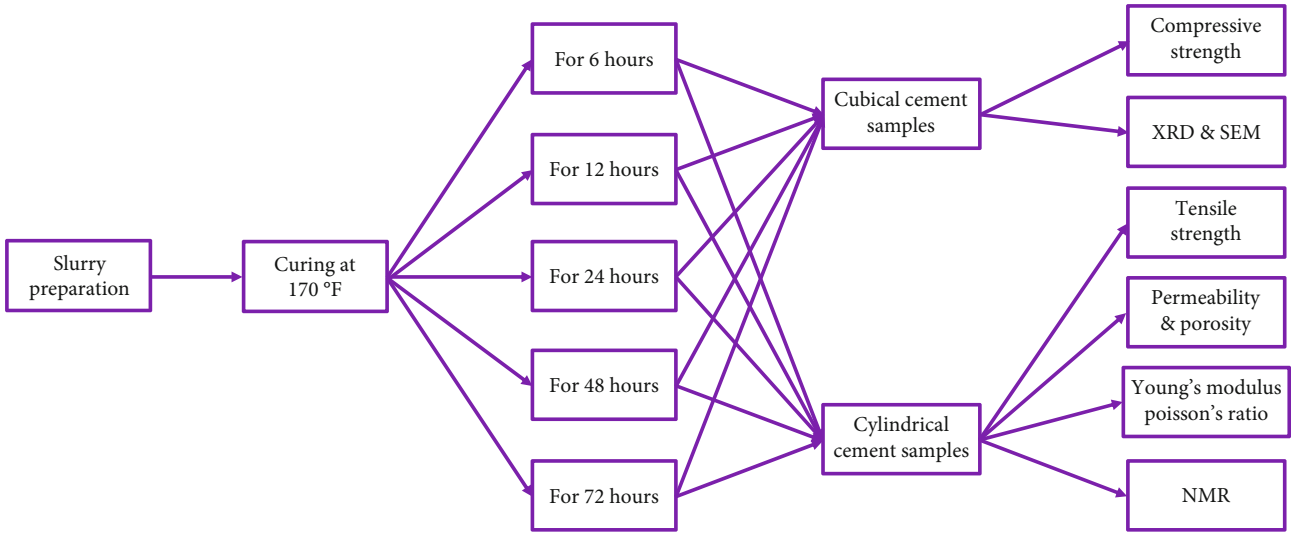

Figure 3: Experimental program.

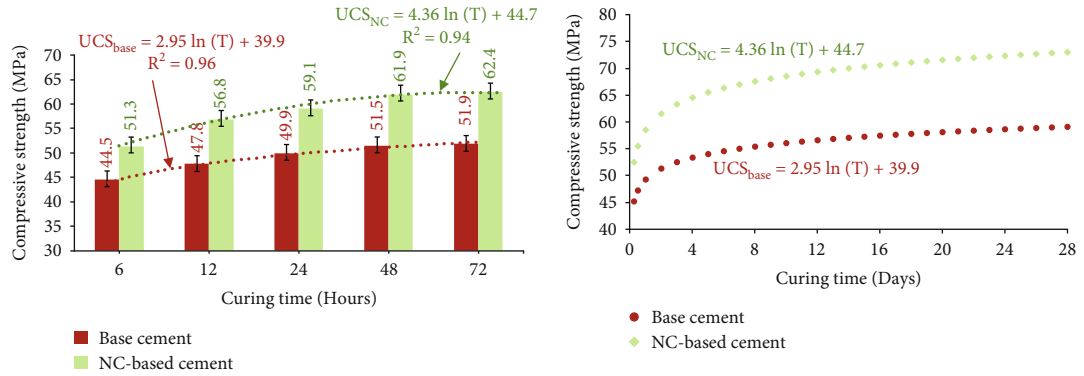

Figure 4: The compressive strength of the nanoclay and base specimens measured at different stages of the curing process.

detector, a reflection-transmission spinner sample stage, and a Cu generator with K-alpha1 [Å] = 1.54060 and K-alpha2 [Å] =1.54443. The minimum step size was set at 0.01°, and the system operated at a current of 40 mA and 45 kV volts. To prepare the samples for XRD measurement, they were finely ground into a powder form.

For the SEM analysis, the cement samples were fractured into small pieces and prepared in a way that allows for SEM analysis by mounting the samples onto a stub using a conductive adhesive such as carbon tape. To increase the conductivity and reduce charging effects during SEM imaging, the samples were coated with a thin layer of conductive material, such as gold, using a sputter coater. After the samples were prepared and coated, they were loaded into the SEM and imaged under high vacuum conditions. Different imaging modes were used to visualize different features of the sample, such as secondary electron imaging (SEI) for surface morphology, backscattered electron imaging (BEI) for compositional contrast, and energy dispersive X-ray spectroscopy (EDS) for elemental analysis. Then, the SEM images and EDS spectra were analyzed to obtain information about the microstructure, composition, and properties of the cement samples.

3. Results and Discussion

3.1. The Effect on the Failure Parameters. The variations in compressive strength of the nanoclay and control (base) cement specimens assessed at several times of curing for 72 hours are summarized in Figure 4. There was a clear increase in the early compressive strength for the nanoclay and control specimens at longer curing times. In this way, the hardened cement's compressive strength is directly related to the curing time. At 48 hours of hydration, there was no appreciable change in the compressive strength of any cement system.

Figure 4(a) demonstrates that when compared to the control specimens, the ones reinforced with nanoclay particles have greater strength. At 6 hours of curing, the compressive strength of the control and nanoclay specimens was 44.5 MPa and 51.3 MPa, respectively. At 48 hours, the compressive strength of the nanoclay and control cement

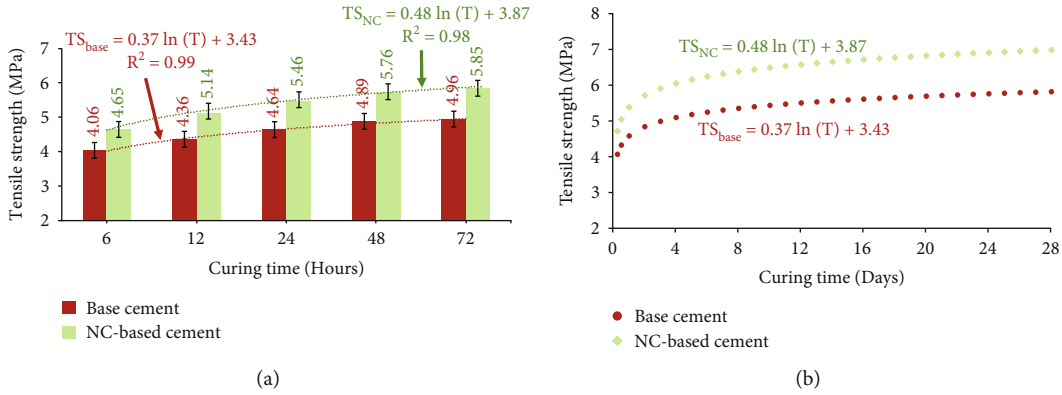

Figure 5: The tensile strength of the nanoclay and base specimens measured at different stages of the curing process.

specimens had stabilized at approximately 51.5 MPa and 61.9 MPa. Both samples showed a small change in compressive strength at 48 hours. Because of the high calcium content of cement, the pozzolanic reaction will be stimulated by the nanoclay's components. This reaction between cement and nanoclay results in the production of calcium silicate hydrate (CSH) crystals, which will improve the compressive strength [51, 52].

Over time, the compressive strength of both systems varies, and this variation was studied analytically to determine the optimal relationship to describe these changes. Logarithmic relationships of (1) and (2), with R^2 values of 0.96 and 0.94, respectively, best characterize the variations in compressive strength for the nanoclay and control cement specimens, as demonstrated in Figure 4(a).

$$\mathrm{UCS}_{\mathrm{base}} = 2.95\ \ln(T) + 39.3, \tag{1}$$

$$\mathrm{UCS}_{\mathrm{NC}} = 4.36\ \ln(T) + 44.7. \tag{2}$$

To compare the compressive strength variations between the two systems over a period of 28 days, (1) and (2) were used (Figure 4(b)). Compressive strength for the nanoclay and control cement specimens changed significantly over the first 7 days of curing, as seen in Figure 4(b). During the first week of hydration, there were only minor variations in compressive strength for the nanoclay and control cement specimens, and by the 21st day, the strength had nearly stabilized.

Figure 5 displays the tensile strength results, and it can be seen that the tensile strength changes are consistent with the compressive strength changes for the nanoclay and control cement specimens. Wherein, as curing time increases, tensile strength also increases. During the first 72 hours of curing, the tensile strengths of the nanoclay samples were higher than those of the control samples.

Figure 5(a) displays that the control and nanoclay cement specimens have a tensile strength of 4.06 MPa and 4.65 MPa, respectively, at 6 hours of curing. At just 48 hours of curing, the tensile strength of the control and nanoclay cement specimens had increased to their respective stabilizing values of 4.89 MPa for the control specimen and 5.76 MPa for the nanoclay specimen. After that point, there was essentially no difference in tensile strength between the two cement samples. Also, the improvement in the compressive and tensile strength for the samples prepared with nanoclay with the curing time is more than that for the base (control) cement, this is attributed to the higher calcium silicate hydrate content in the nanoclay cement samples compared to the base cement and the increase in the CSH in the nanoclay cement samples with time as will be discussed later in this paper. It can therefore be inferred, based on the failure results, that nanoclay cement is favorable for strength improvement.

Regression analysis (shown in Figure 5(a)) demonstrated that the logarithmic relationships of (3) and (4) accurately characterized the variation in tensile strength of the control and nanoclay cement specimens. The R^2 values for these relationships were 0.99 and 0.98, respectively.

$$\mathrm{TS}_{\mathrm{base}} = 0.37\ \ln(T) + 3.43, \tag{3}$$

$$\mathrm{TS}_{\mathrm{NC}} = 0.48\ \ln(T) + 3.87. \tag{4}$$

Changes in tensile strength during the first 28 days of hydration for the control and nanoclay cement specimens were plotted using (3) and (4), as revealed in Figure 5(b). The majority of the tensile strength development in the control and nanoclay cement specimens occurred within the first week of curing, with the tensile strength practically tending to stabilize at 3 weeks for the control specimens and at 24 days for the nanoclay specimens.

3.2. The Effect on the Petrophysical Properties. Figure 6 displays the variation in permeability as curing time increases. In this figure, it can be seen that the permeability of both the control and nanoclay cement specimens decreases with curing time; furthermore, the permeability of the nanoclay cement samples decreases more than that of the control specimens along the curing time, which can be attributed to the nanoclay's ability to fill the microcracks present in the cement matrix. Figure 6(a) shows that the permeability of the control cement and nanoclay cement specimens was 0.059 mD and 0.042 mD, respectively, at 6 hours of curing. At 12 hours, the permeability of both the base cement and the nanoclay cement samples had decreased to 0.047 mD

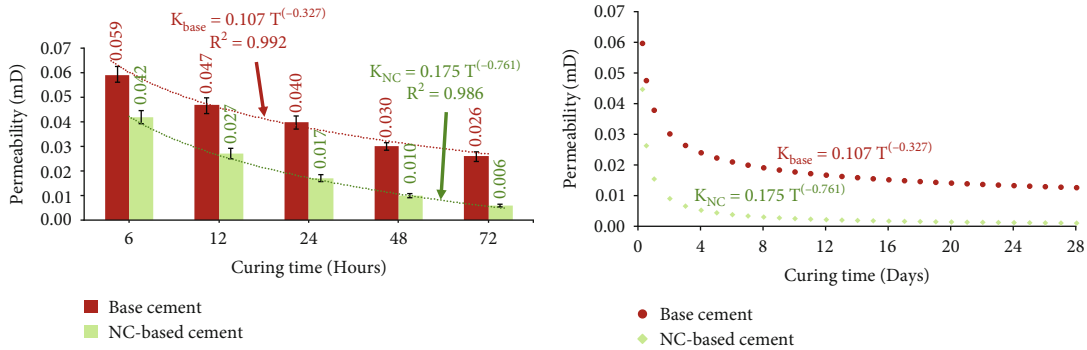

Figure 6: The permeability of the nanoclay and base specimens measured at different stages of the curing process.

and 0.027 mD, respectively. At three days of hydration, the control sample's permeability had decreased to 0.026 mD, while the nanoclay cement sample's permeability had decreased to 0.006 mD. The main reason for the nanoclay cement samples to have less permeability and porosity is that the microcracks do not present in the nanoclay cement samples due to the pore-filling effect of the nanoclay particles which leads to filling the microcracks and preventing their occurrence, as will be discussed in Section 3.5.

Additionally, a mathematical investigation was conducted to identify the most suitable relationship for representing the changes in the permeability of the control and nanoclay cement specimens over time. The analysis revealed that the power relationships of equations (5) and (6), with R^2 values of 0.992 and 0.986, respectively, accurately capture the permeability variations for the base and nanoclay cement samples (refer to Figure 6(a)).

$$K_{base} = 0.107\ T^{-0.327}, \tag{5}$$

$$K_{NC} = 0.175\ T^{-0.761}. \tag{6}$$

Figure 6(b) illustrates the results of applying (5) and (6) to determine the permeability changes that occurred in the control and nanoclay cement specimens during the first 4 weeks of hydration. The result demonstrates that during 7 days, the permeability of the control and nanoclay cement specimens dropped significantly. Until the end of the third week, the permeability was decreasing, although at a slower rate than during the first week of curing. Both samples' permeability stabilized at curing for 24 days.

Cement samples from both systems were analyzed for changes in porosity at 6, 12, 24, 48, and 72 hours of curing, and the results are summarized in Figure 7. The porosity of the samples made with the control and the nanoclay increased as the curing time increased. At 6 hours of hydration, the base (control) samples' porosity was 15.3%; at 48 hours, it had increased significantly to 21.2%. As can be seen in Figure 7(a), the porosity of the nanoclay cement samples began at 10.2% at 6 hours of hydration and increased to 14.9% at two days of curing. At two days of hydration, there was little to no difference in porosity between the two systems, while at three days of curing, the porosity of control and nanoclay cement samples reached 21.6% and 15.3%, respectively. Based on the petrophysical data, it can be deduced that the nanoclay cement sample is preferable because it has lower permeability and porosity than the base sample. Matrix densification in the nanoclay cement occurs as a result of the rapid filling of the space between cement grains by hydrated phases, which speeds up the increase in compressive strength and reduces the petrophysical properties of the nanoclay cement matrix [53–55].

The results of a regression analysis presented in Figure 7(a) demonstrate that the logarithmic relationships of equations (7) and (8) effectively capture the variation in porosity of the control and nanoclay cement specimens. The R^2 values for these relationships are 0.97 and 0.95, respectively.

$$\varnothing_{base} = 2.58\ \ln(T) + 11.0, \tag{7}$$

$$\varnothing_{NC} = 2.01\ \ln(T) + 7.13. \tag{8}$$

Changes in porosity over the first 28 days of hydration for the control and nanoclay cement specimens were plotted using equations (7) and (8), as revealed in Figure 7(b). The figure displays that the porosity of the control and nanoclay cement specimens significantly increased as curing time increased during the first week of hydration. At 24 days of hydration, the rate of increase slowed, and the porosity stabilized, which is consistent with the permeability results.

3.3. NMR Results. The NMR results corroborated the findings from the direct measurement method, demonstrating that the porosity of the samples increases with increasing curing time for both systems. For example, the porosities of the control cement samples at 6, 12, 24, 48, and 72 hours of curing (Figure 8(a)) were 27.4%, 29.7%, 33.1%, 35.2%, and 35.3%, respectively. The nanoclay cement samples followed the same pattern (Figure 8(b)), with porosities of 24.1%, 26.9%, 29.8%, 33.3%, and 34.4% for the 6, 12, 24, 48, and 72 hours of curing samples, respectively. While the porosity values obtained from nuclear magnetic resonance (NMR) differ from those obtained using a gas porosimeter due to variations in measurement techniques, it is evident from Figure 7 that they exhibit a similar pattern. Specifically,

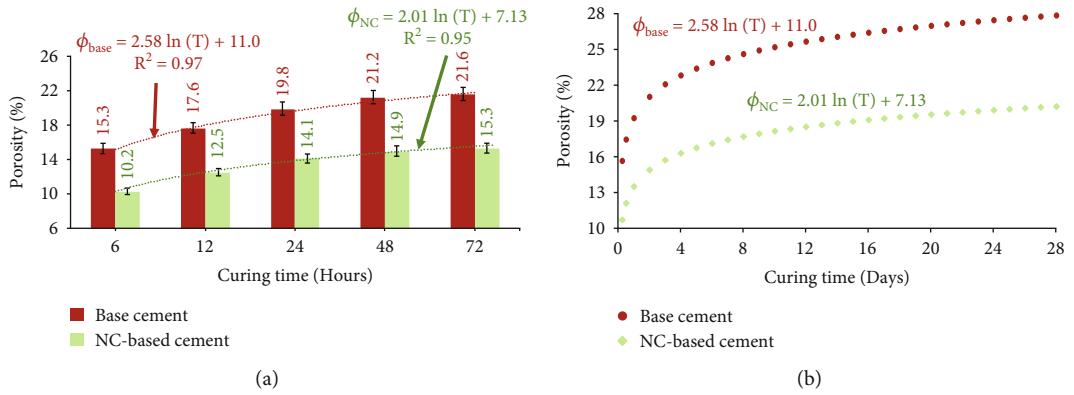

Figure 7: The porosity of both nanoclay and base specimens measured at different stages of the curing process.

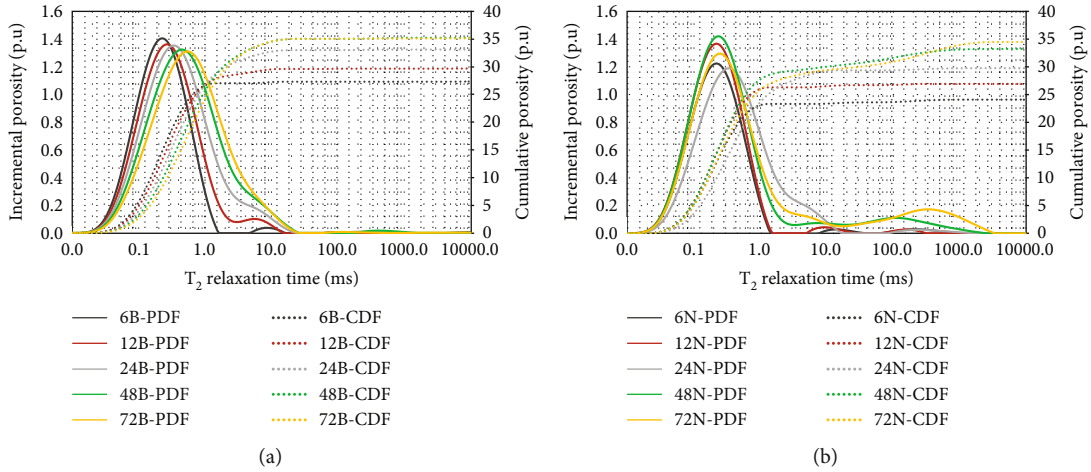

Figure 8: NMR T_2 relaxation for (a) control specimens and (b) nanoclay specimens at 6, 12, 24, 48, and 72 hours of curing.

porosity increases with longer curing time, and the porosities of nanoclay cement are lower compared to the porosity of control cement, despite the discrepancy in measurement methods. Moreover, one can argue that the porosity should be reduced with the curing time. However, it should be pointed out that this is correct for the period after 28 days. According to Farhana et al. [56], the porosity achieved higher values at one-week curing time but further reduced after 4 weeks curing due to the solidification of the structure after 4 weeks which leads to a reduction in the pore spaces. Kumar et al. [57] stated that firstly porosity obtained higher values for one week of curing and later reduced with time. For example, after 4 weeks, the porosity values reduce with the time of curing. After 4 weeks, hydration's heat aggravates and hydrated products fill up the pore spaces that cause the reduction in the porosity.

3.4. The Effect on Elastic Properties. It is generally agreed that the two most crucial elastic properties of solids are Young's modulus and Poisson's ratio. A high Young's modulus indicates more cement's stability under shear stress, and a low Poisson's ratio indicates low expandability [58].

Figure 9 depicts the change in Young's modulus as a function of curing time for specimens of control and nanoclay cement. Young's modulus of the control and nanoclay cement increased with time as curing progressed, but Young's modulus of the nanoclay cement specimens was consistently lower than that of the base samples. Figure 9(a) displays Young's modulus of the control specimen (20.7 GPa) and the nanoclay cement sample (20.3 GPa) at 12 hours of curing. During curing, Young's modulus steadily increased to a maximum value of 21.5 GPa for the control cement specimen and 21.1 GPa for the nanoclay cement specimen at three days of curing. Additionally, it is clear from Young's modulus results that the addition of 1.0% nanoclay reduced the stability of the cement under shear forces as indicated by the decrease in Young's modulus for the samples prepared with 1.0% nanoclay.

It was also mathematically explored to identify the most appropriate relationship to describe the variations in Young's modulus of the control and nanoclay cement specimens with curing time. As can be seen in Figure 9(a), the power relationships of (9) and (10) best describe the variations in Young's modulus for the control and nanoclay cement specimens, with R^2's of 0.998 and 0.980, respectively.

$$E_{s,\text{base}} = 19.7\, T^{0.021}, \tag{9}$$

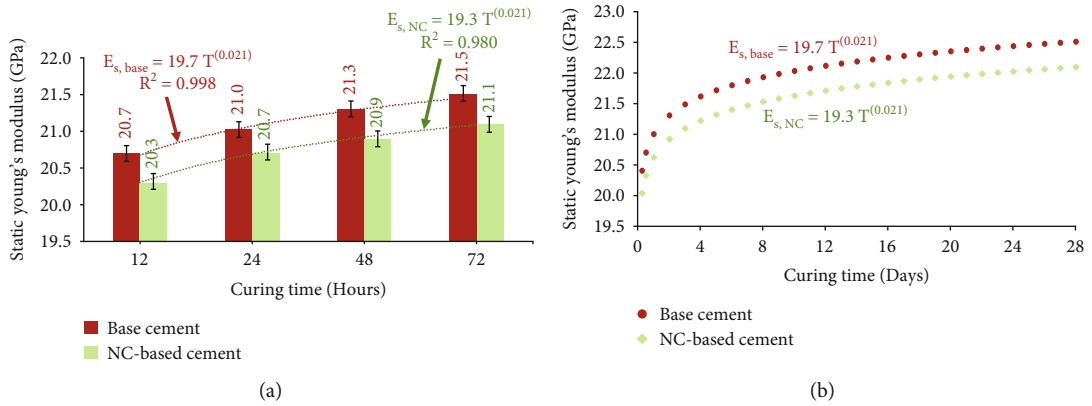

FIGURE 9: Young's modulus values for the nanoclay and base specimens measured at different stages of the curing process.

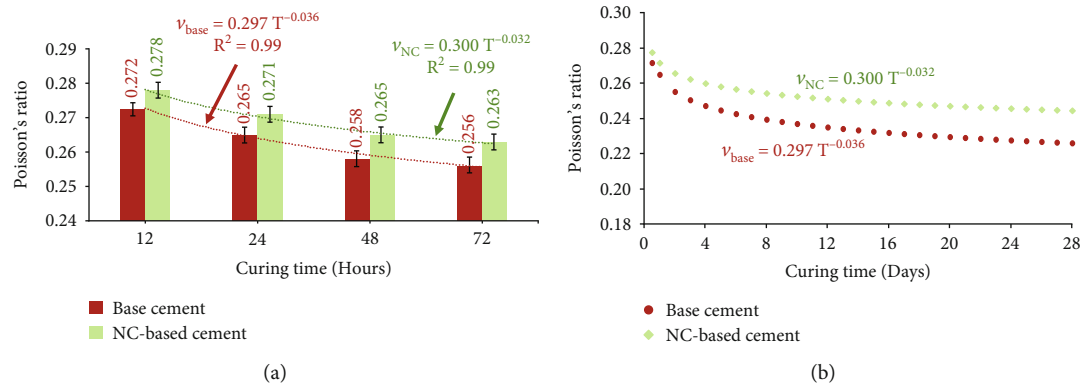

FIGURE 10: Poisson's ratio values for the nanoclay and base specimens recorded at different stages of the curing process.

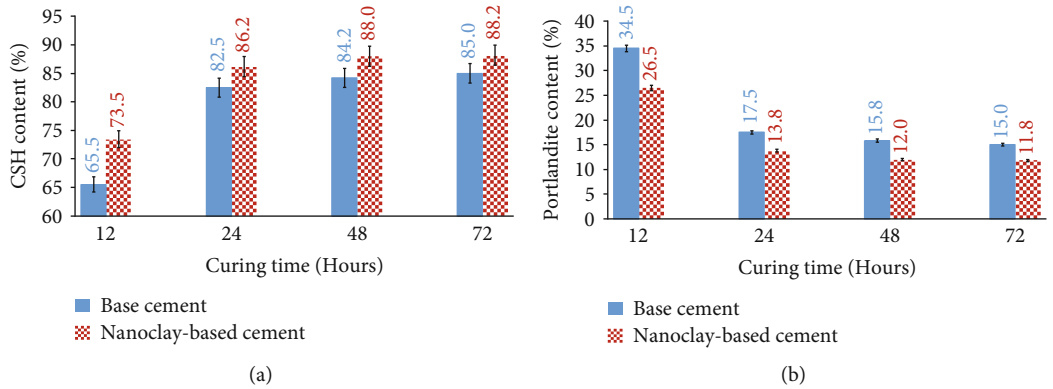

FIGURE 11: XRD results of the amorphous and portlandite content in the cement specimens at 12, 24, 48, and 72 hours of curing.

$$E_{s,NC} = 19.3\ T^{0.021}. \quad (10)$$

Then, using (9) and (10) enables us to determine the variations in Young's modulus of the control and nanoclay cement specimens over the first 4 weeks of hydration. Both cement systems' Young's modulus increased noticeably within the first week, as depicted in Figure 9(b). When compared to the first week of curing, the rate at which Young's modulus increased during the subsequent 23 days was relatively slow. Both samples reached a steady state for Young's modulus at curing for 24 days.

Figure 10(a) shows that at 12 hours of curing, the control cement's Poisson's ratio had reached 0.272, while the nanoclay cement's Poisson's ratio had reached 0.278. At 72 hours of curing, Poisson's ratio of the control and nanoclay cement specimens decreased to 0.256 and 0.263,

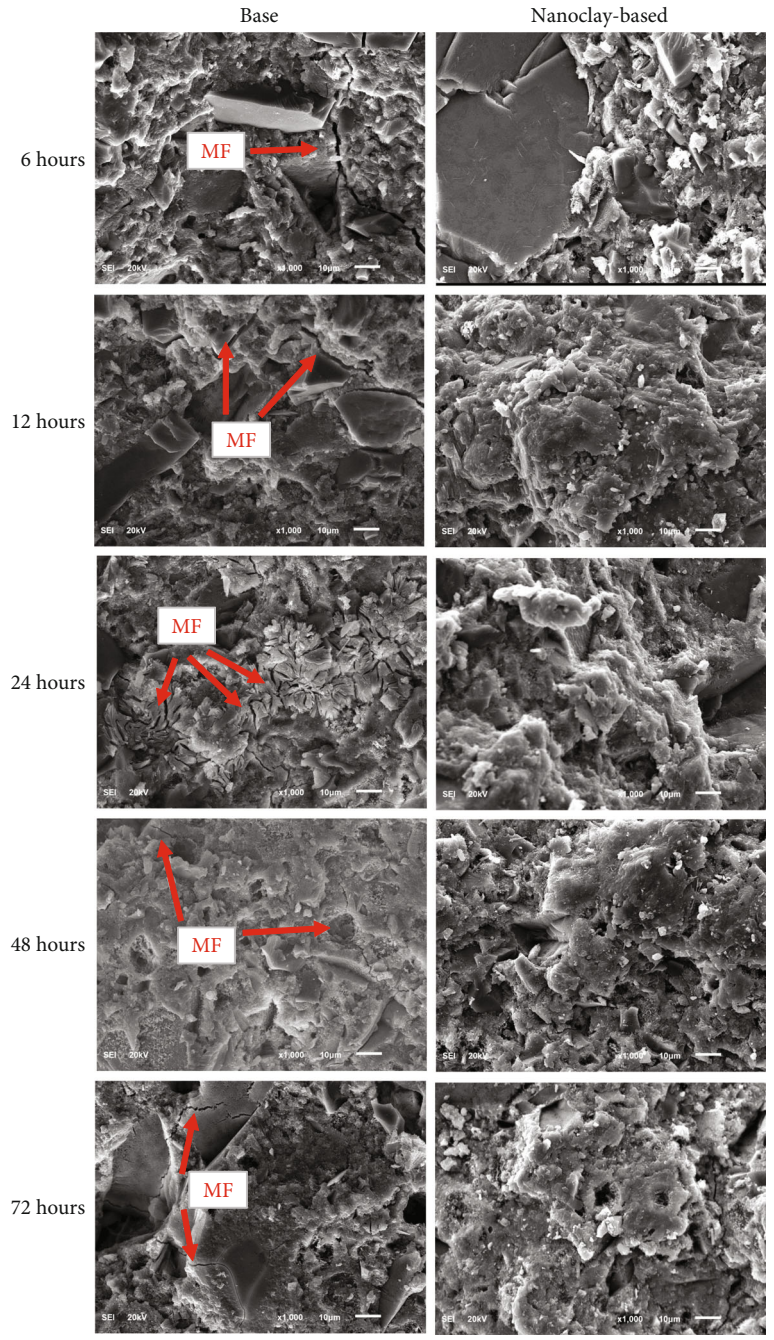

Figure 12: SEM results for the microstructure of the cement specimens at 12, 24, 48, and 72 hours of curing. MF denotes microfractures.

respectively. Figure 10(a) shows that at all curing times, Poisson's ratio for the nanoclay-based cement specimens was greater than that of the base (control) samples, indicating that these samples had high lateral expandability. This finding is consistent with what was previously shown in Figure 9(a) regarding the effects of varying Young's modulus. Overall, the samples' behavior across all curing times indicates that adding nanoclay particles to the cement slurry negatively affects the sheath's elasticity and ability to expand.

Regression analysis was employed to assess the changes in Poisson's ratio over time during the curing process for both the control and nanoclay specimens. The objective was to identify the most suitable mathematical relationship to describe these variations. The findings indicated that the power relationships defined by equations (11) and (12) yielded the best representation of Poisson's ratio variations for the control and nanoclay specimens, respectively. These results were corroborated by the high R^2 value of 0.99. This information is visually depicted in Figure 10(a).

$$\upsilon_{\text{base}} = 0.297\, T^{-0.036}, \tag{11}$$

$$v_{NC} = 0.300\, T^{-0.032}. \quad (12)$$

Figure 10(b) shows the results of using (11) and (12) to determine Poisson's ratio changes that occurred in the control and nanoclay cement specimens during the first 4 weeks of hydration. Figure 10(b) demonstrates a significant decrease in Poisson's ratio for the control and nanoclay cement specimens between 12 hours and 1 week of hydration. Poisson's ratio kept dropping until about halfway through the fourth week at a slower rate than in the first week. Poisson's ratio of the control and nanoclay cement specimens stabilized at 24 days of curing.

3.5. Mineralogical Composition and Microstructural Analysis. The impact of curing time on the structure of the hydrated cement was investigated by characterizing samples of cement at 12, 24, 48, and 72 hours of curing using XRD. The amount of crystalline phases in the cement samples was determined by grounding the cement samples into very fine powder. Then, X-rays were directed onto the cement samples, and the X-rays that were diffracted by the sample were detected and analyzed. The XRD pattern obtained from the cement samples provided information about the crystal structure and phase composition of the sample, in which the intensity of the diffracted X-rays is related to the amount of each crystalline phase present in the sample. The amount of each phase was quantified by comparing the intensity of the diffracted X-rays to a standard reference material. Once the amount of each phase was quantified, the percentage of each phase was calculated based on the total amount of crystalline material present in the sample.

Variations in the amount of CSH and portlandite with curing time for the control and nanoclay specimens are shown by XRD in Figure 11. Figure 11(a) shows that at all stages of curing, the CSH content of the nanoclay cement specimens is greater than that of the control specimens, while the portlandite content of the control specimens is greater (Figure 11(b)). Curing time increased the amorphous content in the two cement systems (Figure 11(a)), while portlandite decreased (Figure 11(b)).

Because nanoclay particles are so rich in silica, they naturally contain a greater concentration of CSH. Due to the silica flour content in the control specimens and both silica flour and nanoclay powder in the nanoclay cement specimens, the portlandite content in both types of samples gradually decreases over time as the pozzolanic reaction proceeds. The increased strength and better elasticity observed in nanoclay cement samples can be traced back to their higher CSH content and decreased portlandite content.

The alteration of the cement matrix microstructure throughout the hydration process through the first three days of curing was also investigated for both cement systems under study, the results of microstructure change are presented in Figure 12. As indicated in this figure at all curing times, the control cement samples are dominated by the presence of microcracks; these microcracks do not present in the nanoclay cement samples and this is because of the pore-filling effect of the nanoclay particles which lead to filling the microcracks and prevent their occurrence. This is the main reason that the nanoclay cement samples have less permeability and porosity. During the hydration process, the interaction between silicon, iron, aluminum, and calcium ions leads to form different compounds of CSH. Where the nanoclay's aluminum reacts with the cement's calcium silicate hydrate (CHS), the cement's chemical behavior and properties are significantly altered and improved [59–63].

4. Conclusions

In this study, a novel work has been conducted by investigating the influence of nanoclay powder on the change of the early properties of class G oil well cement. Cement samples containing nanoclay powder and neat cement samples (without nanoclay powder) were cured at five separate curing processes lasting 6, 12, 24, 48, and 72 hours each, after which the changes in their characteristics were assessed. All the cement specimens were analyzed by three methods namely NMR, XRD, and SEM to understand the change in cement properties as a function of curing time. The results lead to the following conclusions:

(i) The incorporation of the nanoclay particles increased the compressive and tensile strengths of the cement by 20.2% and 17.9%, respectively. This is because of the high CSH content in the nanoclay cement samples as confirmed by the XRD results

(ii) Incorporation of the nanoclay particles reduced the permeability of the cement by 76.9%, and this is attributed to the pore-filling effect of the nanoclay particles as indicated by the presence of the microcracks in the base (control) samples which did not notice in the nanoclay cement samples as confirmed by the SEM results

(iii) The porosity obtained using the NMR agreed with that obtained from the gas porosimeter in which the nanoclay cement samples had lower porosity (29.2% reduction) compared to the control specimens

(iv) The addition of the nanoclay particles reduced Young's modulus by 1.8% and increased Poisson's ratio by 2.7% compared to the control specimens

(v) The compressive strength, tensile strength, porosity, and Young's modulus of the two cement systems (control and nanoclay) increased with the curing time. While the permeability and Poisson's ratio of the control and nanoclay cement specimens decreased with the curing time

Nomenclatures

DV: Density variation (%)
E_s: Static Young's modulus (GPa)
K: Permeability (mD)
NC: Nanoclay
ϕ: Porosity (%)

T: Curing time (hours) (MPa)
TS: Tensile strength (MPa)
UCS: Unconfined compressive strength
v: Poisson's ratio.

Acronyms

°F: Degree Fahrenheit
μm: Micrometre
Al: Aluminum
API: American Petroleum Institute
ASTM: American Society for Testing and Materials
BWOC: By weight of cement
C_2S: Dicalcium silicate
C_3A: Tricalcium aluminate
C_3S: Tricalcium silicate
C_4AF+2C_3A: Tetracalcium aluminoferrite plus twice tricalcium aluminate
Ca: Calcium
CDF: Cumulative distribution function
CSH: Calcium silicate hydrate
Fe: Iron
mD: Millidarcy
MHz: Megahertz
MPa: Megapascal
NMR: Nuclear magnetic resonance
O: Oxygen
PDF: Pore distribution function
PSD: Particle size distribution
R^2: Correlation coefficients
SEM: Scanning electron microscopy
Si: Silicon
T_2: Relaxation time
XRD: X-ray diffraction
XRF: X-ray fluorescence
(w/c): Water-to-cement ratio.

Data Availability

Most of the data are included in the manuscript.

Conflicts of Interest

The authors declare that they have no conflicts of interest.

References

[1] E. B. Nelson and D. Guillot, *Well Cementing*, Schlumberger, 2nd edition, 2006.

[2] K. Krakowiak, J. Thomas, S. Musso, S. James, A. Akono, and F. Ulm, "Nano-chemo-mechanical signature of conventional oil-well cement systems: effects of elevated temperature and curing time," *Cement and Concrete Research*, vol. 67, pp. 103–121, 2015.

[3] G. Collodetti, P. J. Gleize, and P. J. Monteiro, "Exploring the potential of siloxane surface modified nano-SiO2 to improve the Portland cement pastes hydration properties," *Construction and Building Materials*, vol. 54, no. 54, pp. 99–105, 2014.

[4] A. Griffin, J. J. Kim, M. K. Rahman, M. Mahmoud, and R. Taha, "Microstructure of a type G oil well cement-nanosilica blend," *Journal of Materials in Civil Engineering*, vol. 27, no. 5, article 04014166, 2015.

[5] A. S. Griffin, M. K. Rahman, J. J. Kim, and M. R. Taha, "The significance of nanosilica on degradation of oil well cement in carbonated brine environments," in *Ninth international conference on creep, shrinkage, and durability mechanics*, CONCREEP-9, Cambridge, Massachusetts, USA, 2013.

[6] J. J. Kim, M. K. Rahman, and R. Taha, "Examining microstructural composition of hardened cement paste cured under high temperature and pressure using nanoindentation and 29Si MAS NMR," *Applied Nanoscience*, vol. 2, no. 4, pp. 445–456, 2012.

[7] J. H. Moon, M. R. Taha, K. S. Youm, and J. J. Kim, "Investigation of pozzolanic reaction in nanosilica-cement blended pastes based on solid-state kinetic models and 29Si MAS NMR," *Materials*, vol. 9, no. 2, p. 99, 2016.

[8] S. Chithra, S. S. Kumar, and K. Chinnaraju, "The effect of colloidal nano-silica on workability, mechanical and durability properties of high performance concrete with copper slag as partial fine aggregate," *Construction and Building Materials*, vol. 113, pp. 794–804, 2016.

[9] S. Kawashima, P. Hou, D. J. Corr, and S. P. Shah, "Modification of cement-based materials with nanoparticles," *Cement and Concrete Composites*, vol. 36, no. 36, pp. 8–15, 2013.

[10] V. Ershadi, T. Ebadi, A. R. Rabani, L. Ershadi, and H. Soltanian, "The effect of nanosilica on cement matrix permeability in oil well to decrease the pollution of receptive environment," *International Journal of Environmental Science and Development*, vol. 2, no. 2, pp. 128–132, 2011.

[11] R. Patil and A. Deshpande, "Use of nanomaterials in cementing applications," in *Paper presented at the SPE international oilfield nanotechnology conference and exhibition*, SPE-155607-MS, 2012.

[12] L. Senff, D. Hotza, W. L. Repette, V. M. Ferreira, and J. A. Labrincha, "Mortars with nano-SiO2 and micro-SiO2 investigated by experimental design," *Construction and Building Materials*, vol. 24, no. 8, pp. 1432–1437, 2010.

[13] Y. Xu, M. Liu, P. Li et al., "Effect of dispersant types on the rheological and mechanical properties of oil well cement paste with nanosilica," *Construction and Building Materials*, vol. 271, p. 121576, 2021.

[14] P. D. McElroy, H. Emadi, M. C. Watson, and L. Heinze, "Hydration products and mechanical properties investigations of nanofiber additives in cement wellbore environments," SPE Western Regional Meeting. Society of Petroleum Engineers, 2021.

[15] M. T. Baig, M. K. Rahman, and A. Al-Majed, "Application of nanotechnology in oil well cementing," in *Paper presented at the SPE Kuwait oil & gas Show and conference*, SPE-187543-MS, Kuwait City, Kuwait, 2017.

[16] M. K. Rahman, W. A. Khan, M. A. Mahmoud, and P. Sarmah, "MWCNT for enhancing mechanical and thixotropic properties of cement for HPHT applications," in *Paper presented at the offshore technology conference Asia, Kuala Lumpur, Malaysia*, OTC-26465-MS, 2016.

[17] A. Dinesh, B. Abirami, and G. Moulica, "Carbon nanofiber embedded cement composites: properties and promises as sensor – a review," *Materials Today: Proceedings*, vol. 44, pp. 4166–4172, 2021.

[18] Z. Ren, Y. Liu, L. Yuan et al., "Optimizing the content of nano-SiO2, nano-TiO2 and nano-CaCO3 in Portland cement paste

by response surface methodology," *Journal of Building Engineering*, vol. 35, article 102073, 2021.

[19] D. Wang, X. Yao, T. Yang, W. Xiang, Y. Feng, and Y. Chen, "Controlling the early-age hydration heat release of cement paste for deep-water oil well cementing: a new composite designing approach," *Construction and Building Materials*, vol. 285, article 122949, 2021.

[20] M. K. Moraes and E. Maria da Costa, "Effect of adding organo-modified montmorillonite nanoclay on the performance of oil-well cement paste in CO2-rich environments," *Cement and Concrete Composites*, vol. 127, article 104400, 2022.

[21] K. Mei, L. Zhang, Y. Wang et al., "Structural evolution in nanoclay reinforced Oilwell cement during supercritical co2 (SCCO2) invasion," *IOP Conference Series: Earth and Environmental Science*, vol. 861, no. 7, article 072002, 2021.

[22] A. O. Arinkoola, K. K. Salam, S. O. Alagbe, A. S. Afolayan, and I. U. Duru, "Influence of metakaolin and nano-clay on compressive strength and thickening time of class G oil well cement," *Songklanakarin Journal of Science and Technology*, vol. 43, no. 1, pp. 118–126, 2022.

[23] M. A. Sanjuán, C. Argiz, J. C. Gálvez, and A. E. Moragues, "Effect of silica fume fineness on the improvement of Portland cement strength performance," *Construction and Building Materials*, vol. 96, pp. 55–64, 2015.

[24] A. Hakamy, F. U. A. Shaikh, and I. M. Low, "Characteristics of hemp fabric reinforced nanoclay-cement nanocomposites," *Cement and Concrete Composites*, vol. 50, no. 50, pp. 27–35, 2014.

[25] A. Hakamy, F. U. A. Shaikh, and I. M. Low, "Characteristics of nanoclay and calcined nanoclay-cement nanocomposites," *Composites Part B: Engineering*, vol. 78, pp. 174–184, 2015.

[26] M. Stefanidou and I. Papayianni, "Influence of nano-SiO2 on the Portland cement pastes," *Composites Part B: Engineering*, vol. 43, no. 6, pp. 2706–2710, 2012.

[27] A. A. Mahmoud, S. Elkatatny, A. Ahmed, and M. Mahmoud, "Nanoclay content influence on cement strength for oil wells subjected to cyclic steam injection and high-temperature conditions," in *Paper presented at the Abu Dhabi International Petroleum Exhibition & Conference*, SPE-193059-MS, Abu Dhabi, UAE, 2018.

[28] M. Murtaza, M. Rahman, and A. Al Majed, "Effect of nanoclay on mechanical and rheological properties of oil well cement slurry under HPHT environment," in *Paper presented at the international petroleum technology conference*, IPTC-18989-MS, Bangkok, Thailand, 2016.

[29] A. A. Mahmoud, S. Elkatatny, A. Ahmed, and R. Gajbhiye, "Influence of nanoclay content on cement matrix for oil wells subjected to cyclic steam injection," *Materials*, vol. 12, no. 9, 2019.

[30] S. Ma, T. Yu, Y. Wang, M. Chaouche, and S. Kawashima, "Phase evolution of oil well cements with nano-additive at elevated temperature/pressure," *ACI Materials Journal*, vol. 113, no. 5, pp. 571–578, 2016.

[31] S. Ma and S. Kawashima, "A rheological approach to study the early-age hydration of oil well cement: effect of temperature, pressure and nanoclay," *Construction and Building Materials*, vol. 215, pp. 119–127, 2019.

[32] Z. Tariq, M. Murtaza, and M. Mahmoud, "Effects of nanoclay and silica flour on the mechanical properties of class G cement," *ACS Omega*, vol. 5, pp. 11643–11654, 2020.

[33] A. S. Mohammed, "Vipulanandan model for the rheological properties with ultimate shear stress of oil well cement modified with nanoclay," *Egyptian Journal of Petroleum*, vol. 27, no. 3, pp. 335–347, 2018.

[34] M. I. Miah, S. Ahmed, S. Zendehboudi, and S. Butt, "Machine learning approach to model rock strength: prediction and variable selection with aid of log data," *Rock Mechanics and Rock Engineering*, vol. 53, no. 10, pp. 4691–4715, 2020.

[35] J. W. Carey, M. Wigand, S. J. Chipera et al., "Analysis and performance of oil well cement with 30 years of CO2 exposure from the SACROC unit, West Texas, USA," *International Journal of Greenhouse Gas Control*, vol. 1, no. 1, pp. 75–85, 2007.

[36] N. Agofack, S. Ghabezloo, J. Sulem, A. Garnier, and C. Urbanczyk, "Experimental investigation of the early-age mechanical behaviour of oil-well cement paste," *Cement and Concrete Research*, vol. 117, pp. 91–102, 2019.

[37] M. J. Thiercelin, B. Dargaud, J. F. Baret, and W. J. Rodriguez, "Cement design Besed on cement mechanical response," in *Paper presented at the SPE annual technical conference and exhibition*, SPE-38598-MS, San Antonio, Texas, 1997.

[38] H. Justnes, D. Van Loo, B. Reyniers, J. Skalle, P. Sveen, and E. J. Sellevold, "Chemical shrinkage of oil well cement slurries," *Advances in Cement Research*, vol. 7, no. 26, pp. 85–90, 1995.

[39] S. K. Lyomov, K. R. Backe, P. Skalle, O. B. Lile, H. Justnes, and J. Sveen, "Shrinkage of oil well cement slurries," in *Paper presented at the annual technical meeting*, PETSOC-97-77, Calgary, Alberta, 1997.

[40] P. A. Parcevaux and P. H. Sault, "Cement shrinkage and elasticity: a new approach for a good," in *Paper presented at the SPE annual technical conference and exhibition*, SPE-13176-MS, Houston, Texas, 1984.

[41] L. Reinås, H. Hodne, and A. T. Mirkamil, "Hindered strength development in oil well cement due to low curing temperature," in *Paper presented at the SPE Arctic and Extreme Environments Conference and Exhibition*, SPE-149687-MS, Moscow, Russia, 2011.

[42] L. J. Parrott, M. Geiker, W. A. Gutteridge, and D. Killoh, "Monitoring Portland cement hydration: comparison of methods," *Cement and Concrete Research*, vol. 20, no. 6, pp. 919–926, 1990.

[43] G. Sant, M. Dehadrai, D. Bentz et al., "Detecting the fluid-to-solid transition in cement pastes, comparing experimental and numerical techniques," *Concrete International-A contribution from ACI Commit-tee*, vol. 236, pp. 53–58, 2009, https://www.dora.lib4ri.ch/empa/islandora/object/empa%3A2456.

[44] A. Ahmed, A. A. Mahmoud, and S. Elkatatny, "The effect of polypropylene fiber on the curing time of class G oil well cement and its mechanical, petrophysical, and elastic properties," *Journal of Petroleum Exploration and Production Technologies*, vol. 13, no. 4, pp. 1181–1196, 2023.

[45] K. Sobolev and M. F. Gutierrez, "How nanotechnology can change the concrete world - part one," *American Ceramic Society Bulletin*, vol. 84, no. 2005, pp. 14–17, 2009.

[46] J. J. Thomas, H. M. Jennings, and J. J. Chen, "Influence of nucleation seeding on the hydration mechanisms of tricalcium silicate and cement," *The Journal of Physical Chemistry C*, vol. 113, no. 11, pp. 4327–4334, 2009.

[47] API, *Worldwide Cementing Practices*, API, Dallas, Texas, USA, 1991.

[48] API, *API Recommended Practice 10B-2-Recommended Practice for Testing Well Cements*, American Petroleum Institute, Washington, Second edition, 2013.

[49] ASTM, *C109/C109M. Standard Test Method for Compressive Strength of Hydraulic Cement Mortars (Using 2-in. Or [50-Mm] Cube Specimens)*, ASTM International, West Conshohocken, PA, USA, 2016, http://www.astm.org/.

[50] ASTM, *D3967-16, Standard Test Method for Splitting Tensile Strength of Intact Rock Core Specimens*, ASTM International, West Conshohocken, PA, 2016, http://www.astm.org/.

[51] S. K. Amin, M. E. Allam, G. L. Garas, and H. A. Ezz, "A study of the chemical effect of marble and granite slurry on green mortar compressive strength," *Bulletin of the National Research Centre*, vol. 44, no. 1, p. 19, 2020.

[52] J. Doneliene, A. Eisinas, K. Baltakys, and A. Bankauskaite, "The effect of synthetic hydrated calcium aluminate additive on the hydration properties of OPC," *Advances in Materials Science and Engineering*, vol. 2016, Article ID 3605845, 8 pages, 2016.

[53] B. Jo, C. Kim, G. Tae, and J. Park, "Characteristics of cement mortar with nano-SiO2 particles," *Construction and Building Materials*, vol. 21, no. 6, pp. 1351–1355, 2007.

[54] A. Korpa, R. Trettin, K. G. Böttger, J. Thieme, and C. Schmidt, "Pozzolanic reactivity of nanoscale pyrogene oxides and their strength contribution in cement-based systems," *Advances in Cement Research*, vol. 20, no. 1, pp. 35–46, 2008.

[55] G. Land and D. Stephan, "The influence of nano-silica on the hydration of ordinary Portland cement," *Journal of Materials Science*, vol. 47, no. 2, pp. 1011–1017, 2012.

[56] Z. F. Farhana, H. Kamarudin, A. Rahmat, and A. M. Mustafa Al Bakr, "The relation between water absorption and porosity for geopolymer paste," *Material Science*, vol. 803, pp. 166–172, 2015.

[57] M. H. Kumar, I. S. Macharyulu, T. Ray et al., "Effect of water absorption and curing period on strength and porosity of triple blended concrete," *Materials Today: Proceedings*, vol. 43, pp. 2162–2169, 2021.

[58] E. Fjaer, R. M. Holt, P. Horsrud, A. M. Reean, and R. Risnes, *Petroleum Related Rock Mechanics*, Elsevier Science, 2nd edition, 2007.

[59] A. R. Brough, A. Katz, G. K. Sun, L. J. Strubl, R. J. Kirkpatrick, and J. F. Young, "Adiabatically cured, alkali-activated cement-based wasteforms containing high levels of fly ash," *Cement and Concrete Research*, vol. 31, no. 10, pp. 1437–1447, 2001.

[60] S. Y. Hong and F. P. Glasser, "Alkali sorption by C-S-H and C-A-S-H gels," *Cement and Concrete Research*, vol. 32, no. 7, pp. 1101–1111, 2002.

[61] I. G. Richardson, "The nature of C–S–H in hardened cements," *Cement and Concrete Research*, vol. 29, no. 8, pp. 1131–1147, 1999.

[62] I. G. Richardson and J. G. Cabrera, "The nature of C–S–H in model slag-cements," *Cement and Concrete Composites*, vol. 22, no. 4, pp. 259–266, 2000.

[63] J. Schneider, M. A. Cincotto, and H. Panepucci, "29 Si and 27Al high resolution NMR characterization of calcium silicate hydrate phases in activated blast-furnace slag pastes," *Cement and Concrete Research*, vol. 31, pp. 993–1001, 2001.